Flux loss distributions due to breakup in the elastic scattering of 56 MeV deuterons from ^{51}V

A. Ingemarsson,[1,2] B. R. Karlsson,[2] and R. Shyam[3]
[1]*The Svedberg Laboratory, Box 533, S-75121 Uppsala, Sweden*
[2]*Department of Radiation Sciences, Box 535, S-75121 Uppsala, Sweden*
[3]*Saha Institute of Nuclear Physics, Calcutta 700 064, India*
(Received 9 October 2001; published 23 April 2002)

The loss of flux from the elastic channel due to breakup is calculated in a model case (56 MeV deuterons on ^{51}V) where the breakup contribution to the imaginary part of the nucleus-nucleus optical potential has been explicitly determined. We find that most of the flux is lost in a cap-shaped region near the nuclear surface while a smaller part is lost at a refractive focus.

DOI: 10.1103/PhysRevC.65.054604 PACS number(s): 24.10.Eq, 24.10.Ht, 25.45.−z, 25.60.Gc

I. INTRODUCTION

In the scattering of composite particles, the breakup of the projectile is a dominant reaction channel. Within a theory of the breakup reactions formulated in the framework of the post-form distorted wave Born approximation (PFDWBA) [1], a good understanding has been achieved of the experimental data on the breakup reaction induced by the light projectiles (with mass numbers $\leqslant 4$). One of the assumptions of this theory is that breakup reactions are sensitive to the extreme surface region of the target nuclei. Already in 1947 Serber [2] predicted that the breakup of the deuteron takes place at the grazing distance from the target nucleus.

In a recent publication [3], the elastic and inelastic breakup cross sections calculated within the PFDWBA theory were used as constraints to determine the contributions to the imaginary part of the deuteron optical potential due to the breakup channels. In this method only the first order breakup process (the coupling of the elastic channel to the breakup channel) is considered and the unitarity of the S matrix is used to determine the influence of breakup on the elastic channel. It was noted that this potential accounted for most of the absorption in the surface region of the target nucleus, however, the region where the breakup potentials peak was found to be much larger than the half density radius deduced by Serber [2]. It is, therefore, of interest to do a more detailed study of the pattern of the flux loss from the elastic channel, due to the breakup process.

It has been shown in Refs. [4,5] that a better understanding of the properties of the scattering process can be obtained by studying the full scattering wave function and the associated quantum flux. The divergence of the flux associated with the scattering wave function gives a measure of the localization of nonelastic processes that deplete the entrance channel. A study of this quantity corresponding to the breakup channels is expected to provide valuable information about the location of the loss of flux due to the breakup process. [6].

In this paper we have studied the total scattering wave function and the divergence of the quantum flux due to the breakup channels. Our aim is to pinpoint more precisely the region where the loss of flux due to the breakup channels takes place. In the following section, we describe the method of calculations briefly. The results of our calculations are presented in Sec. III. The summary and conclusions of our work are given in Sec. IV.

II. QUANTUM FLUX DUE TO THE BREAKUP CHANNELS

The breakup reaction, like other inelastic processes, entails a loss of flux from the incident channel. The continuity equation for the probability density $\rho(\mathbf{r},t)$ in the elastic channel, therefore, contains an absorptive term, and in a local optical potential model one has

$$\frac{\partial}{\partial t}\rho(\mathbf{r},t)-\boldsymbol{\nabla}\cdot\mathbf{j}(\mathbf{r},t)=-\frac{2}{\hbar}W(r)\rho(\mathbf{r},t), \tag{1}$$

where $W(r)$ is the imaginary part of the optical potential, $\rho(\mathbf{r},t)$ is the probability density, and $j(\mathbf{r})$ is the quantum flux. Ignoring the time dependence, we can write

$$\boldsymbol{\nabla}\cdot\mathbf{j}(\mathbf{r})=-\frac{2}{\hbar}W(r)\rho(\mathbf{r}). \tag{2}$$

In Eq. (2), $\rho(\mathbf{r})=|\Psi^{(+)}(\mathbf{r})|^2$, where $\Psi^{(+)}(\mathbf{r})$ is the full optical model wave function. It will be assumed here that the inelastic processes take place where the flux is lost, i.e., the loss term on the right hand side of Eq. (1) also describes where, in the nuclear volume, the inelastic processes occur. This assumption is consistent with the expression for the reaction cross section

$$\sigma_R=\frac{1}{\hbar v}\int W(r)|\Psi^{(+)}(\mathbf{r})|^2 d\mathbf{r}. \tag{3}$$

σ_R is the experimentally accessible measure of the total loss of flux from the elastic channel. Detailed investigations of the integrand in Eq. (3) were recently reported by Brau *et al.* [5] and Ingemarsson *et al.* [7].

The reaction cross section can be expressed as a sum over partial wave transmission coefficients (T_l),

$$\sigma_R=\frac{\pi}{k^2}\sum_l (2l+1)T_l, \tag{4}$$

where $\hbar k$ is the relative momentum and the transmission coefficient T_l is given by

$$T_l = \frac{4}{\hbar v} \int |y_l(r)|^2 W(r) dr. \tag{5}$$

In Eq. (5), $y_l(r)$ is the radial part of the total wave function.

Using unitarity of the S matrix, the transmission coefficient T_l can be written as

$$T_l = 1 - |S_l|^2 = \sum_{c \neq l} |S_{l_c}|^2, \tag{6}$$

where S represents the scattering matrix and l denotes the elastic channel. Thus Eq. (6) enables us to express the transmission coefficient T_l as a sum (or integral for continuous channels) over all the reaction channels. This allows us to write

$$\sigma_R = \sigma_R^{bare} + \sigma_{bu}, \tag{7}$$

for each partial wave l. In this equation σ_{bu} represents the contribution to the reaction cross section from the breakup channels, while σ_R^{bare} is the reaction cross section corresponding to the remaining channels. Following Refs. [8,9], the imaginary part of the optical potential may be decomposed into a bare component and a component due to breakup as $W(r) = W_{bare}(r) + W_{bu}(r)$. Then, expressions similar to Eq. (4) can be written for σ_R^{bare} and σ_{bu}, with corresponding transmission coefficients being given by

$$T_l^{bare} = \frac{4}{\hbar v} \int |y_l(r)|^2 W_{bare}(r) dr, \tag{8}$$

and

$$T_l^{bu} = \frac{4}{\hbar v} \int |y_l(r)|^2 W_{bu}(r) dr. \tag{9}$$

W_{bu} consists of a part due to elastic breakup (W_{diss}) and a part due to the inelastic breakup (W_{inbu}). We determine these potentials by fitting the elastic and inelastic breakup cross sections calculated within the PFDWBA (see, e.g., Ref. [3] for a detailed discussion).

As an extension of the previous considerations, it will be assumed that if the loss term on the right hand side of Eq. (1) is decomposed in a similar manner, then each term describes where in the nuclear volume the corresponding process occurs. In particular, it will be assumed that the term $(W_{bu}(r)|\Psi^{(+)}(\mathbf{r})|^2)$ reveals where the breakup of the projectile takes place. A direct investigation of the distribution of flux loss in the scattering volume, as represented by the integrand in Eq. (3), is expected to provide [5,7] insight into the breakup process that complements, and transcends, such a partial wave or impact parameter analysis.

It should be remarked that the flux loss distributions, obtained as outlined above, will depend on the reaction model. The calculations reported below have all been performed with local optical potentials. Effects of nonlocality may be important, particularly, in the nuclear interior. However, as we are considering processes that are centered mostly around the nuclear surface, we believe that at least the gross features of our results are of a general nature.

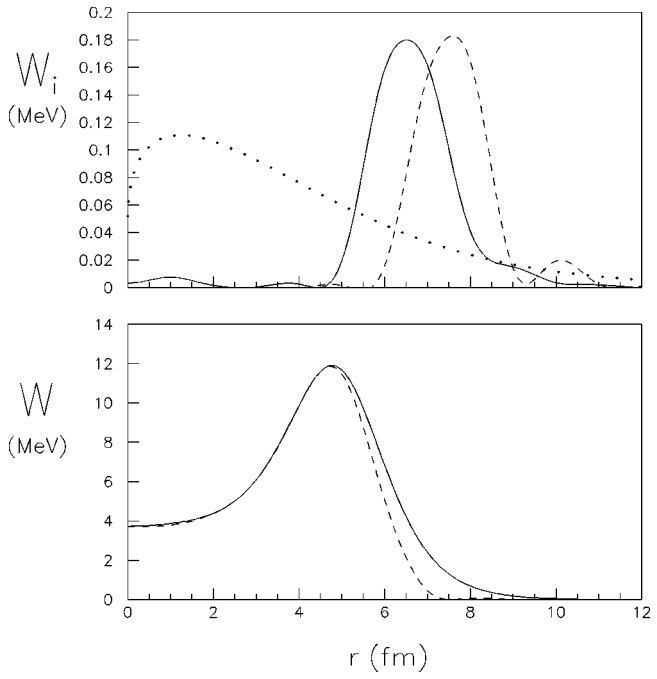

FIG. 1. The upper figure shows the contributions to the imaginary potential from inelastic breakup, multiplied by 0.09 to fit in the plot (solid curve), from elastic breakup (dashed curve), and from Coulomb dissociation (dotted curve). The lower part shows the imaginary potential with (solid curve) and without (dashed curve) effects of breakup.

III. RESULTS AND DISCUSSIONS

As a model case, we consider the scattering of 56 MeV deuterons on ^{51}V, since for this system a decomposition of the optical potential was worked out recently by Ingemarsson and Shyam [3]. The optical potential was taken from the global sets given by Daehnick, Childs, and Vrcelj [10]. In addition, a weak breakup potential with very long range was added in order to simulate the effects of the Coulomb dissociation at large distances. The results for the imaginary potentials are shown in Fig. 1 (which are the same as those shown in Ref. [3]). The upper part shows the imaginary potentials due to the inelastic breakup (solid line), the nuclear dissociation (dashed line), and the Coulomb dissociation (dotted line). The inelastic breakup potential has been plotted after multiplying the actual numbers by 0.09. The lower part shows the total imaginary potential with (solid line) and without (dashed line) effects of the breakup terms.

The probability density $\rho(\mathbf{r}) = |\Psi^{(+)}(\mathbf{r})|^2$ is invariant under rotations about the forward direction (the z axis), and it can, therefore, be illustrated as a distribution over the xz plane, as is shown in the top panels of Fig. 2. Since, in the case considered here, the real part of the optical potential is strongly focused, a sharp maximum appears in $|\Psi^{(+)}(\mathbf{r})|^2$, some 4.5 fm behind the center of the nucleus (top left panel). At larger distances, there is an enhancement also in the forward direction. In the right panels, the effect of switching off the real part of the potential (V) is shown. It can be clearly seen that both the structures mentioned above disappear, leaving behind an almost ''dark'' shadow region.

To present these effects more clearly, we show, in the

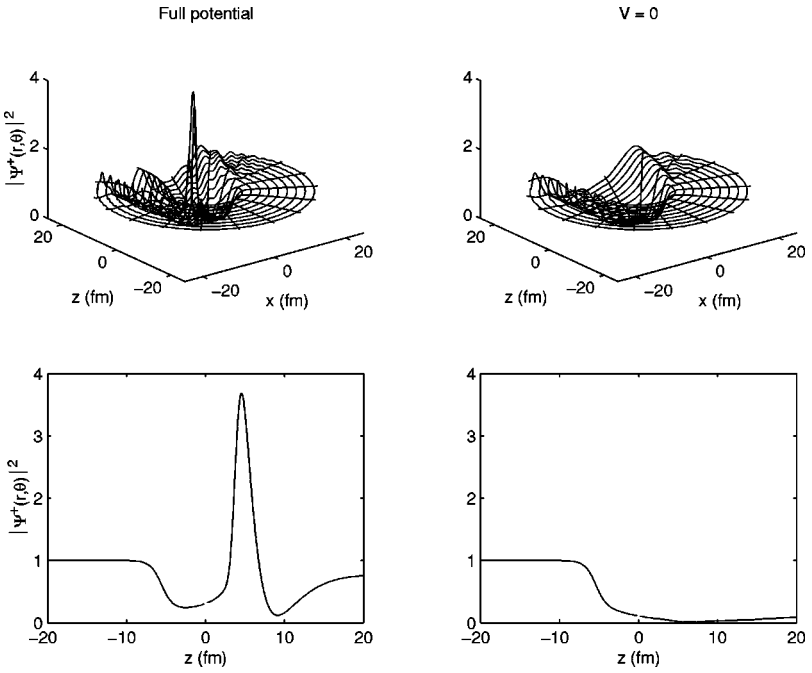

FIG. 2. Values of $|\Psi^{(+)}(\mathbf{r})|^2$ in the elastic scattering of 56 MeV deuterons from ^{51}V in the xz plane. The left parts show the results from calculations with the full potential. The right part shows the results without real potential. The lower part shows the variation of $|\Psi^{(+)}(\mathbf{r})|^2$ along the central trajectory. The direction of the incident beam is along the z axis.

lower part of Fig. 2, a section of the probability densities along the axis of the incident beam (z axis). It can be clearly seen that the focus is localized at about 4.5 fm from the center of the target nucleus for the case of $\rho(\mathbf{r})$ calculated with full potential. The enhancement mentioned above occurs mainly outside the interaction region. Both these effects disappear from the probability density calculated without the real part of the potential.

With known imaginary potentials and wave function, it is now possible to calculate not only the total flux loss distribution, but also the contributions from the three breakup channels (Coulomb dissociation, nuclear dissociation, and inelastic breakup), as outlined above. In Fig. 3, we show the values of $W_i(r)|\Psi^{(+)}(\mathbf{r})|^2$ as distributions in the reaction plane, corresponding to the cases where contributions from all the breakup components are included (top left) along with only inelastic breakup (top right), only elastic nuclear breakup (lower part left), and only Coulomb dissociation (lower part right). Since the large amplitudes at the refractive focus make it difficult to display the characteristic features in the individual cases, the same distributions are also displayed as contour plots, in Fig. 4. An impression of the distribution in three dimensions can be obtained if a contour curve from Fig. 4 is rotated about the z axis. The resulting surfaces limit the regions in space where the absorption (i.e., flux loss density) exceeds a given value, as exemplified in Fig. 5 for the elastic breakup. The contour line corresponds in this case to a value of 30% of the maximum value. The elastic and the inelastic breakup potentials are surface dominated, and the resulting flux loss patterns indicate that these reactions are concentrated in a narrow band (i.e., in a thin cap-shaped region in three dimensions) at a specific radius.

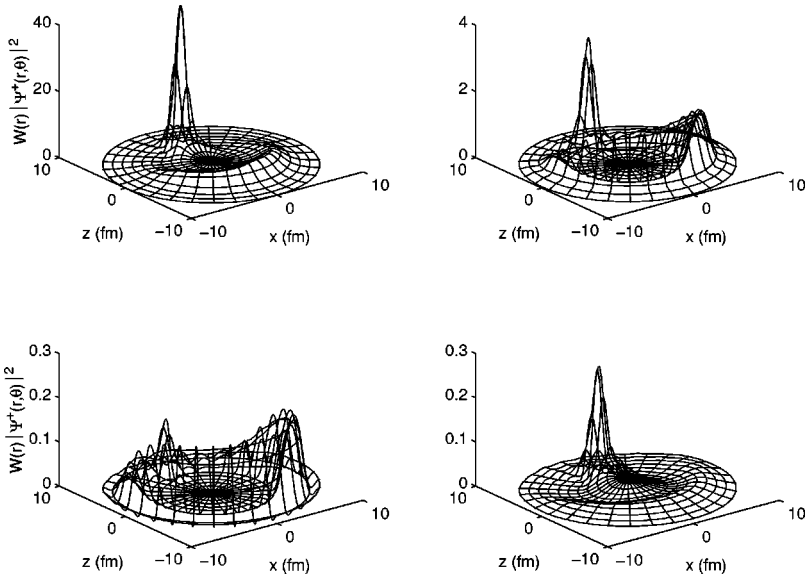

FIG. 3. Values of $W_{bu}(r)|\Psi^+(\mathbf{r})|^2$ in the elastic scattering of 56 MeV deuterons from ^{51}V in the xz plane. The upper left panel includes all contributions to the total reaction cross section. The upper right panel shows the contributions due to inelastic breakup. In the lower part, contributions from elastic nuclear breakup (left) and Coulomb dissociation (right) are shown. The direction of the incident beam is along the z axis.

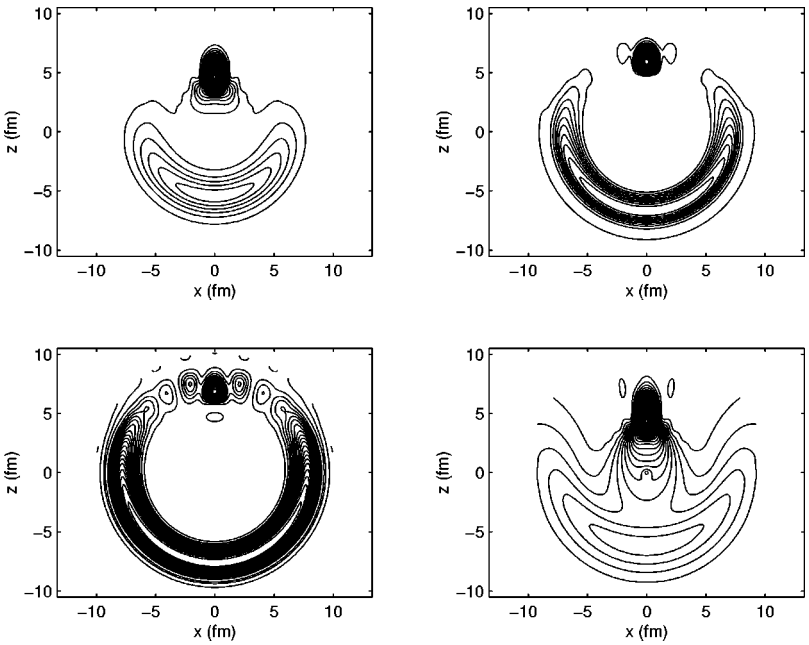

FIG. 4. Contour plots of the values $W_i(r)|\Psi^{(+)}(\mathbf{r})|^2$ shown in Fig. 3.

More specifically, it can be seen that in the elastic case (Fig. 4, down left), the maximum probability for breakup at the front side of the nucleus is almost independent of the impact parameter. For the inelastic breakup, which peaks at a somewhat smaller radius (compare Fig. 1), central collisions are somewhat favored as compared to peripheral ones. In both cases, the width of the breakup region is almost constant as seen from the center of the nucleus.

This picture of breakup reactions in which the process takes place more or less uniformly in a spherical shell on the front side of the nucleus implies that for geometrical reasons the elastic breakup cross section is dominated by contributions from the large partial waves. Indeed, if seen as a function of the impact parameter, the apparent width of the breakup region increases with a geometric factor and the area element in the impact parameter plane increases linearly with l.

The enhancement at the refractive focus is seen in all the cases. However, since it is limited to a small volume, its contribution to σ_R is less conspicuous, and it can also be expected to be sensitive to how nonlocality is dealt with in the reaction model. In any case, its relative importance calls for further investigations, not only about its model dependence but also about its possible experimental signatures.

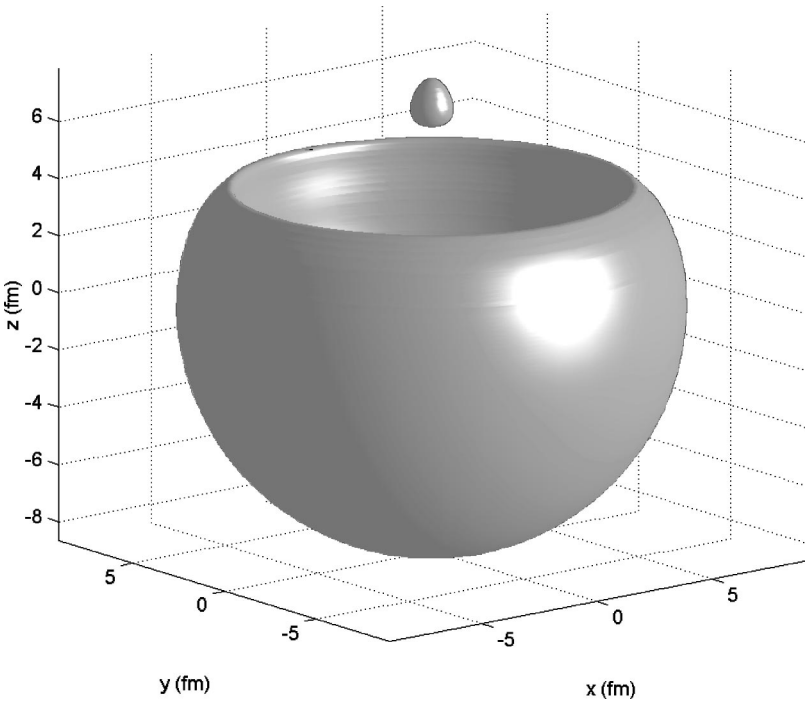

FIG. 5. Three-dimensional plot generated by the contour line at 30% of the maximum value in Fig. 3 for the elastic breakup (down left).

IV. SUMMARY AND CONCLUSIONS

In this paper we calculated the quantum probability density and the divergence of the flux due to the breakup of deuterons on a ^{51}V target at the beam energy of 56 MeV. It is observed that the flux loss distribution due to breakup processes is localized in a narrow cap region near the surface of the target nucleus. This region appears at a larger radius than the half density radius deduced by Serber [2].

[1] G. Baur, R. Shyam, F. Rösel, and D. Trautmann, Helv. Phys. Acta **53**, 506 (1980); G. Baur, F. Rösel, D. Trautmann and R. Shyam, Phys. Rep. **111**, 333 (1984); G. Baur, S. Typel, and H. Wolter, in *Proceedings of the RCNP-TAMU Symposium*, edited by edited by H. Yabu, T. Suzuki, and H. Toki (World Scientific, Singapore, 2000), p. 119; R. Shyam and P. Danielewicz, Phys. Rev. C **63**, 054608 (2001).

[2] R. Serber, Phys. Rev. **72**, 1008 (1947).

[3] A. Ingemarsson and R. Shyam, Phys. Rev. C **60**, 054615 (1999).

[4] I. E. McCarthy, Nucl. Phys. **11**, 574 (1959); Phys. Rev. **128**, 1237 (1962); K. A. Amos, Nucl. Phys. **77**, 225 (1966).

[5] F. Brau, F. Michel, and G. Reidemeister, Phys. Rev. C **57**, 1386 (1998).

[6] A. Kassano and M. Ichimura, Phys. Lett. **115B**, 81 (1982).

[7] A. Ingemarsson, G. J. Arendse, A. Auce, R. F. Carlson, A. A. Cowley, A. J. Cox, S. V. Förtsch, R. Johansson, B. R. Karlsson, M. Lantz, J. Peavy, J. A. Stander, G. F. Steyn, and G. Tibell, Nucl. Phys. **A696**, 3 (2001).

[8] M. S. Hussein, Phys. Rev. C **30**, 1962 (1985).

[9] J. A. Christley, M. A. Nagarajan, and I. J. Thompson, J. Phys. G **17**, L163 (1991).

[10] W. W. Daehnick, J. D. Childs, and Z. Vrcelj, Phys. Rev. C **21**, 1153 (1980).